27th International Congress
on Sound and Vibration
The annual congress of
the International Institute
of Acoustics and Vibration (IIAV)

11-16 July, 2021

ICSV27

Annual Congress of the International Institute of Acoustics and Vibration (IIAV)

THE INFLUENCE OF EDGE GEOMETRY ON END-CORRECTIONS IN MICROSLIT ABSORBERS

Alessia Aulitto, Avraham Hirschberg and Ines Lopez Arteaga
TU/e Eindhoven University of Technology, Eindhoven,The Netherlands
e-mail:a.aulitto@tue.nl

The influence of the edge geometry on the viscous dissipation and inertia in microslit absorbers (MSAs) is investigated. MSAs are plates with arrays of slit-shaped perforations backed by a shallow cavity providing a lightweight solution for acoustic liners. To optimize the viscous dissipation, the slit height and the plate thickness are chosen to be of the order of the acoustic viscous boundary layer thickness *i.e.* in the submillimeter range. Because of the manufacturing process, for these perforations, the edge shape is not always sharp. The acoustic behavior is investigated assuming a slit in a rectangular confinement channel, given by actual walls or by hydrodynamical interactions due to neighboring slits. The flow within the slit is assumed locally incompressible. Viscous dissipation and inertia of the slit are described in terms of resistive and inertial end-corrections. A combination of analytical models and numerical solutions of the incompressible Linearized Navier-Stokes equations is proposed. The effect of the edge geometry is investigated using potential flow theory combined with a thin viscous boundary layer approximation. The analytical model successfully predicts the end-corrections for rounded edges, up to a radius of curvature of the order of the slit height. From this study it emerges that the inertial end-correction of the slit is a global property sensible to the far-field behavior of the flow and strongly dependent on the porosity, unlike observed for circular perforations. On the contrary, the resistive end-correction is a localized phenomenon, weakly dependent on the porosity and dominated by the edge geometry of the perforation.

Keywords: Slit, Microslit, Edge, End-corrections, Absorbers

1. Introduction

Microslit absorbers (MSPs) and plates (MSPs) have been proposed as efficient sound absorbers, providing light-weight and compact solutions for acoustic liners at low frequencies [1]. In simple MSAs the plate is mounted with a shallow backing cavity or a sub-partitioned backing cavity. Alternative designs of MSAs have been reported in the literature [2][3][4]. MSPs are plates with arrays of slits with height in the sub-millimeter range. To optimize viscous dissipation, the slit height is chosen to be of the order of magnitude of a few times the acoustical viscous boundary layer thickness $\delta_v = \sqrt{2\nu/\omega}$, where ν is the kinematic viscosity of air and $\omega = 2\pi f$, with f the frequency. For perforation in the sub-millimeter range, the accuracy of the manufacturing process can not be guaranteed. In particular, the sharpness of

the edge is not always achieved. This problem is common to slits and circular perforations. For a circular perforation, chamfering the edges reduces the effective plate thickness t_{eff} by a length of the order of the total length of the chamfers [5]. This can be also found in [6]. The purpose of this work is to investigate the influence of the edge geometry on the acoustic end-corrections of slits in MSAs. The discussion is limited to the normal incidence of acoustic waves. For a sharp edged slit a model for high Sh_b numbers, based on an incompressible potential flow with a thin boundary layer, is proposed by Morse and Ingard [7]. This model yields both inertial and resistive end-corrections in the limit of high Shear numbers. For a slit in an infinitely thin plate, the same approach does predict an inertial end-correction. However, the singularity of the potential flow at the edge of an infinitely thin plate results in a divergence of the resistive end-correction due to the singularity at the edge [7]. This suggests that the viscous dissipation is a local effect, strongly influenced by the edge geometry. In Section 2, the assumptions are described with formal definition of the impedance and of the end-corrections. Furthermore, the thin boundary layer approximation is used to investigate the end-corrections for smooth edges and for sharp square edges. In Section 3, analytical results are compared to numerical solution of the linearized Navier-Stokes equations for smooth and rounded edges.

2. Theory

2.1 Assumptions, impedance and end-corrections

In a microslit plate, the hydrodynamical interaction between the perforations can be described by considering a single slit of height b in a plate, confined within a channel of rectangular cross-section aw, with a the distance between neighboring slits and w the lateral length of the slit (see Fig.1). The acoustic properties of MSPs are defined by the porosity $\Phi = b/a$, with b being the slit height and a the distance between neighboring slits (confinement channel height). The typical porosity of MSPs is $\Phi = O(1\%)$.

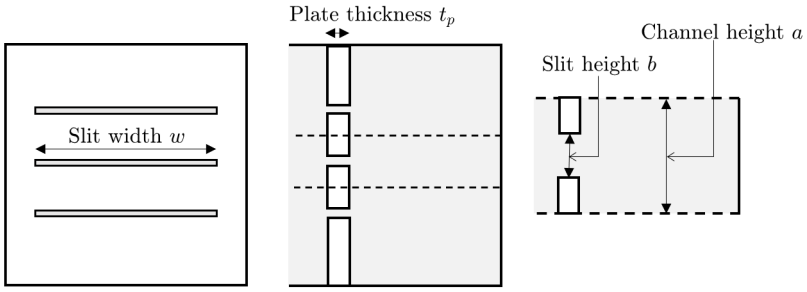

Figure 1: On the left, frontal view of the microslit plate with slit width w. In the middle, lateral view of the microslit plate of thickness t_p with back cavity. On the right, a single single of height b with confinement channel of height a due to hydrodynamic interactions.

Assuming a long slit ($w >> b$) implies that one can consider a two dimensional $(2D)$ acoustical flow through the slit. In the audio range, the square of the Helmholtz number is small, *i.e.* $He^2 = \left(\frac{\omega b}{c}\right)^2 < 10^{-1}$, for slit height b of the order of the millimeter and c the speed of sound. Thermal effects in the slit are neglected [8]. As the slit forms the neck of a Helmholtz resonator with a portion of the back cavity as volume, the flow within the slit can be considered as locally incompressible up to the first resonance frequency of the resonator, $\omega_H = c\sqrt{\Phi/(d_c t_{eff})}$, with d_c the back cavity depth and t_{eff} the plate thickness plus the inertial end-correction. For typical applications of MSAs, the slit height b is of the order of the viscous boundary layer thickness, *i.e.* the Shear number $Sh_b = b/\delta_v$ is of order unity. Given the transition from a slit of height b to a channel of height $a > b$, in an ideal (reference) configuration

this transition is abrupt: the flow can be described as a piece-wise parallel flow. For a long thin slit of height b, width $w >> b$ and length $t_p >> b$, one can assume a parallel flow in the slit and define the slit impedance, Z_b, as

$$Z_b = \frac{\Delta\widehat{p}}{wb < \widehat{u} >}, \tag{1}$$

where $\Delta\widehat{p}$ is the pressure difference between the sides of the slit [1],[8]. In the actual flow, the transition from the slit to the confinement channel is not abrupt. However, far from the transition one can observe the linear change in pressure, corresponding to a parallel flow in a slit of height b and in a confinement channel of height a. This far field can be extrapolated at each side of the transition towards the plate surface at $x = 0$. The complex difference in pressure $\Delta\widehat{p}_t$ obtained across the transition by this extrapolation divided by volume flux amplitude $\widehat{U} =< \widehat{u} > bw$ is defined as the transition impedance Z_t. The inertial end-correction δ_{in} and the resistive end-correction δ_{res} are defined by

$$\delta_{in} = \frac{Im\left[Z_t\right]}{Im\left[\frac{dZ_b}{dt_p}\right]}, \tag{2}$$

$$\delta_{res} = \frac{Re\left[Z_t\right]}{Re\left[\frac{dZ_b}{dt_p}\right]}, \tag{3}$$

where at the denominator one finds the parallel flow impedance per unit length of the slit dZ_b/dt_p. In principle, the resistive end-correction δ_{res} is different from the inertial end-correction but they are both of the order of magnitude of the slit height.

2.2 Slit with smooth edges

For the high Sh_b range, the viscosity effects are concentrated in a thin boundary layer at the wall and do not impact the main, potential flow. An analytical solution is proposed for a smooth transition, providing a generalization of the results for sharp edges in [7]. In Fig. 2, a 2D slit of height b in $x < 0$ and a 2D channel of height $a > b$ in $x > 0$ are shown. The end of the uniform slit (point B in Fig. 2) is

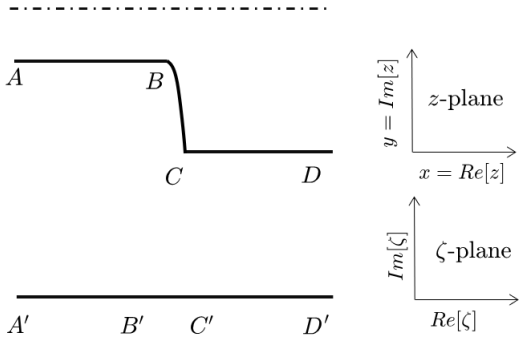

Figure 2: Henrici's transformation of half the channel expansion with smooth transition in the physical plane $z = x + iy$ to the $\zeta-$plane. Coordinates of the points: $A(-\infty; (a+b)/2)$, $B(-d; (a-b)/2)$, $C(0,0)$, $D(\infty; 0)$.

at $(x, y) = (-d, a - b)$, with d being the transition length. The uniform confinement channel begins at $x = 0$. The duct can be associated to a region in the complex $z-$plane by $z = x + iy$, with $i^2 = -1$ and coordinates (x, y). Using conformal mapping, the flow region in the duct can be mapped into the upper

half-plane in the complex $\zeta-$plane. The mapping of the contraction is a modified Schwarz-Christoffel transformation described in [9],[10]. The integral form of the transformation is

$$z = \alpha \left[\ln \frac{1+\tau}{1-\tau} - \frac{1}{G} \ln \frac{G+\tau}{G-\tau} \right] + \beta \ln \left[\frac{\zeta}{G^2} \right], \tag{4}$$

where τ is:

$$\tau = \sqrt{\frac{\zeta - G^2}{\zeta - 1}}. \tag{5}$$

The parameters of the transformation α, β and G depend on the slit and channel heights and on the transition length d. The point far downstream of the transition A can be mapped into point A'($\zeta = 0$), the end of the slit B corresponds to B'($\zeta = 1$), the end of the transition C$(0,0)$ corresponds to C'($\zeta = G^2$). The equation for the sharp square edge transition is recovered for $d = 0$. The inertial and resistive end-corrections can be found comparing the actual configuration to an ideal configuration. The ideal reference flow has for $x > 0$ a uniform velocity u_a in the channel of height a and for $x < 0$ a uniform velocity $u_b = (a/b)u_a$. The potential flow far upstream is obtained by placing a volume source at the origin $\zeta = 0$ (far downstream the transition) with potential $\varphi = (au_a/\pi)\, ln(\zeta)$. The local flow velocity is the vector field $\vec{v}_{wall} = (u, v) = \nabla\varphi$. The linearized form of the frictionless equation of motion is

$$-\nabla p = \rho_0 \frac{\partial \vec{v}}{\partial t}. \tag{6}$$

In order to compare the actual and the reference configurations two points in the transformed $\zeta-$plane are necessary. Choosing $\zeta_1 \to \infty$ and $\zeta_2 = 0$ corresponds to z_1 and z_2 respectively far upstream and far downstream the transition. Integrating Eq. 6 between $z_1 = (x_1; y_1)$ and $z_2 = (x_2; y_2)$ with $x_1 > 0$ and $x_2 < 0$, one has for a harmonic oscillating acoustic field:

$$\mathrm{i}\rho\omega(\varphi_2 - \varphi_1) = p_1 - p_2, \tag{7}$$

with $\varphi = \int \vec{v} \cdot d\vec{z}$. If the flow velocity would remain uniform $(u_a, 0)$ for $x > 0$ and jump to $(u_b, 0)$ with $u_b = u_a a/b$ for $x < 0$, we would have:

$$(\varphi_2 - \varphi_1)_{ideal} = u_a \frac{a}{b} x_2 - u_a x_1. \tag{8}$$

The inertial end-correction δ_{in} is given by

$$\delta_{in} = \frac{u_a a}{b \Delta\varphi}, \tag{9}$$

where $\Delta\varphi = (\varphi_2 - \varphi_1)_{actual} - (\varphi_2 - \varphi_1)_{ideal}$. Choosing real values ζ_1 and ζ_2, so that the values of z_1 and z_2 are far from the origin of the axis, one has:

$$\delta_{in} = \frac{b}{\pi} \ln \left(\frac{\zeta_2}{\zeta_1} \right) - Re(z_2) + \frac{b}{a} Re(z_1). \tag{10}$$

For $\zeta_1 \to \infty$ and $\zeta_2 \to 0$ in Eqs. 4-5, one can expand τ to the first order and obtain an expression for z_1 and z_2 to substitute in Eq. 10, leading to

$$\delta_{in} = \frac{1}{\pi} \left\{ \frac{(a-b)^2}{2ab} \ln \left(\frac{1+G}{1-G} \right) + \frac{a-b}{b(G-1)} \left[\frac{Gb+a}{2a} \ln \left(\frac{(1+G)^2}{4G^2} \right) \right] + \ln G \right\}. \tag{11}$$

For $d = 0$ one recovers the result for sharp edges [7]. In the thin boundary layer approximation the flow in the boundary layer is quasi-parallel along the wall. The additional dissipation due to the transition can be derived integrating along the wall the dissipation per unit surface for the actual and the reference configuration [7]. It should be noted that the actual configuration and the ideal configuration should be combined to obtain converging integrals. In terms of potential the velocity at the wall is

$$|\widehat{u}_{tan}|^2 = \left|\frac{d\varphi}{dz}\right|^2 = \left|\frac{d\varphi}{d\zeta}\right|^2 \left|\frac{d\zeta}{dz}\right|^2. \tag{12}$$

The power dissipated at the junction compared to an ideal configuration is [7]

$$2\vec{P} = \frac{1}{\delta_v}\eta w \left[\int_{\zeta_2}^{\zeta_0} \left(\left|\frac{d\varphi}{d\zeta}\right|^2 \frac{d\zeta}{dz} - u_a^2 * \left(\frac{a}{b}\right)^2 Re\left[\frac{dz}{d\zeta}\right]\right) d\zeta + \int_{\zeta_0}^{\zeta_1} \left(\left|\frac{d\varphi}{d\zeta}\right|^2 \frac{d\zeta}{dz} - u_a^2 Re\left[\frac{dz}{d\zeta}\right]\right) d\zeta\right], \tag{13}$$

where for a symmetric slit $\zeta_1 \to \infty$, $\zeta_2 \to 0$ and ζ_0 corresponds to $z = 0$ and it is found from $\zeta_0 = G^2$. It is interesting to note that, in Eq. 13, the first integral contains the effect of the dissipation in the slit and near the edge, whereas the second integral refers to the walls of the confinement channel. For a slip boundary condition prevailing in a confinement channel resulting from hydrodynamic interactions, one can take $\zeta_1 \to \zeta_0$ and calculate the dissipation using only the first integral. The resistive end-correction of the discontinuity can be defined as [7]:

$$\delta_{res} = \frac{2\vec{P}}{(2awu_a)^2}. \tag{14}$$

Solving the integrals for the smooth-edged configuration with friction at the channel walls leads to

$$\delta_{res} = \frac{(G-1)}{2G(a-b)}\left\{(G-1)\left[\frac{(G+1}{\pi(G-1)}\left(\frac{(a-b)^2}{b^2(G+1)} - 1\right)\ln\left(\frac{G+1}{G-1}\right) + 1\right] - \frac{2DG^2}{\pi}\ln(G)\right\}, \tag{15}$$

with $D = \frac{Gb-a}{G(a-b)}$. Again for $d = 0$ one recovers the result of [7], with $G = a/b$ and $D = 0$.

2.3 Slit with sharp square edges

For a slit with sharp edges ($d = 0$), at low porosity $\Phi = b/a$ the inertial end-correction is proportional to $\ln(1/\Phi)$. Hence, it becomes infinitely large for vanishing porosity. This behaviour is different from the behaviour of inertia for circular perforations found in [11]. The divergence of the inertial end-correction for a slit is due to the failure of the incompressible flow approximation at low He number in 2D unconfined flows. Compressibility effects have been discussed in [12]. However, the inertial end-correction for a slit of height b, for low porosity, will be much larger than for a circular perforation of diameter b. The resistive end-correction increases with decreasing porosity but reaching an asymptotic value of the order b for $\Phi \to 0$. This behaviour is similar to the resistive end-correction for circular perforations found in [13]. The effect of the boundary condition (slip or no-slip) on the channel walls is investigated for a typical porosity $1/\Phi = 10$ with $Sh_b = 2$ and $Sh_b = 20$. Numerical simulations for $1/\Phi = 10$ show that the introduction of a no-slip boundary condition at the walls of the confinement channel has a negligible effect on the results. Using the thin boundary layer theory, for high Sh_b one finds $\delta_{res,no-slip}/\delta_{res,slip} = 1.041$, in agreement with numerical results for $Sh_b = 2$ and $Sh_b = 20$. One expects that this ratio increases for increasing porosity. For an extremely large porosity $1/\Phi = 3$, one finds a ratio $\delta_{res,no-slip}/\delta_{res,slip} = 1.185$. This study confirms that the viscous dissipation is mainly concentrated around the edge.

3. Results

In this section the results of the thin boundary layer approximation for smooth transitions are compared with the results for sharp edges. The reference length L_{ref} is introduced. For Henrici's transformation, $L_{ref} = d$ is the transition length. For round edges $L_{ref} = r$, the radius of curvature of the rounded edge. In Fig. 3, $\delta_{in,round}/\delta_{in,sharp}$ calculated using the high Sh_b number limit, is shown for height ratios a/b relevant in MSPs. The inertial end-correction shows a strong dependency on the porosity that increases with the increase of the ratio L_{ref}/b. The resistive end-correction, in Fig. 4 as $\delta_{res,round}/\delta_{res,sharp}$, shows a much more modest dependency on the porosity. For decreasing porosity the resistive end-correction becomes independent on the porosity.

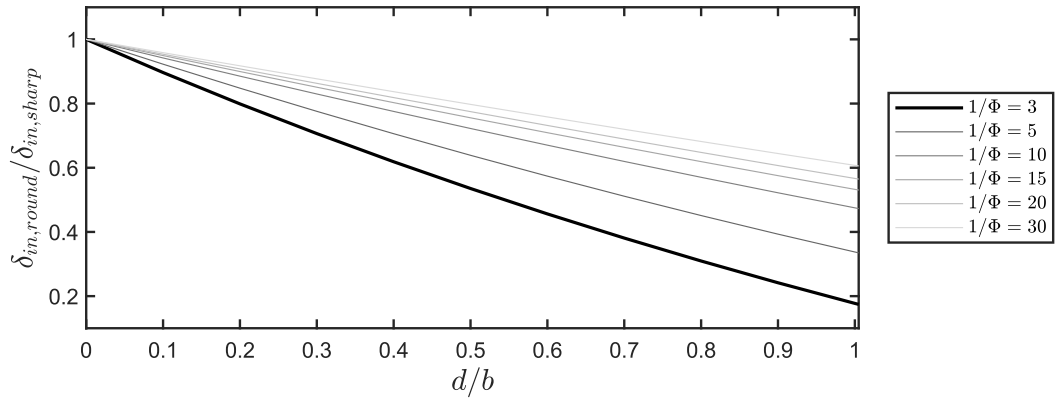

Figure 3: Behavior of $\delta_{in,round}/\delta_{in,sharp}$ as function of the edge rounding L_{ref}/b.

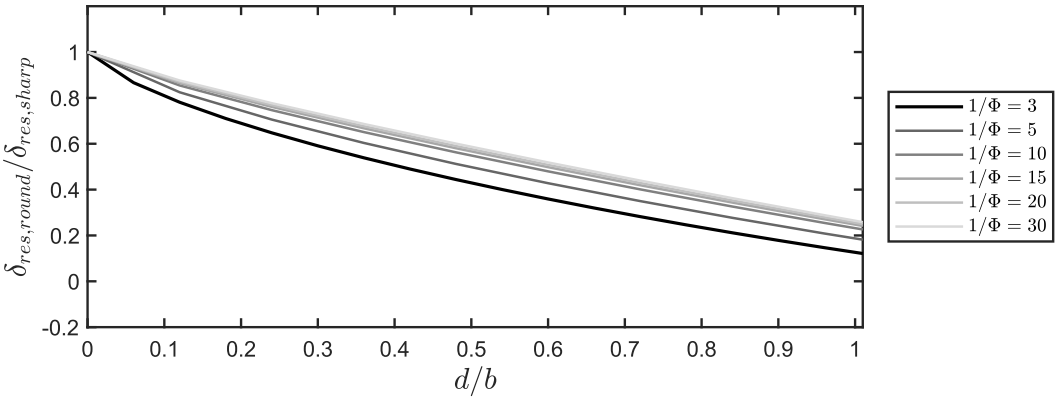

Figure 4: Behavior of $\delta_{res,round}/\delta_{res,sharp}$ as function of the edge rounding L_{ref}/b.

The analytical solution with thin boundary layer for smooth edges is validated by the numerical solutions of the Linearized Navier-Stokes equations (LNSE) for Henrici's geometry at high Sh_b number.

In Fig. 5-6, the end-corrections derived by the analytical model are compared with the numerical results for smooth edges and round edges at $Sh_b = 20$ for $1/\Phi = 10$. Both for the resistive and the inertial end-correction, the analytical solution well approximates the numerical results for a rounded edge when assuming $d = r$ at high Sh_b numbers. The resistive end-correction for a round edge becomes negative for L_{ref}/b of order unity. As a result, one can conclude that the inertial end-correction is affected by the edge geometry but is dominated by the porosity whereas the resistive end-correction strongly depends on the

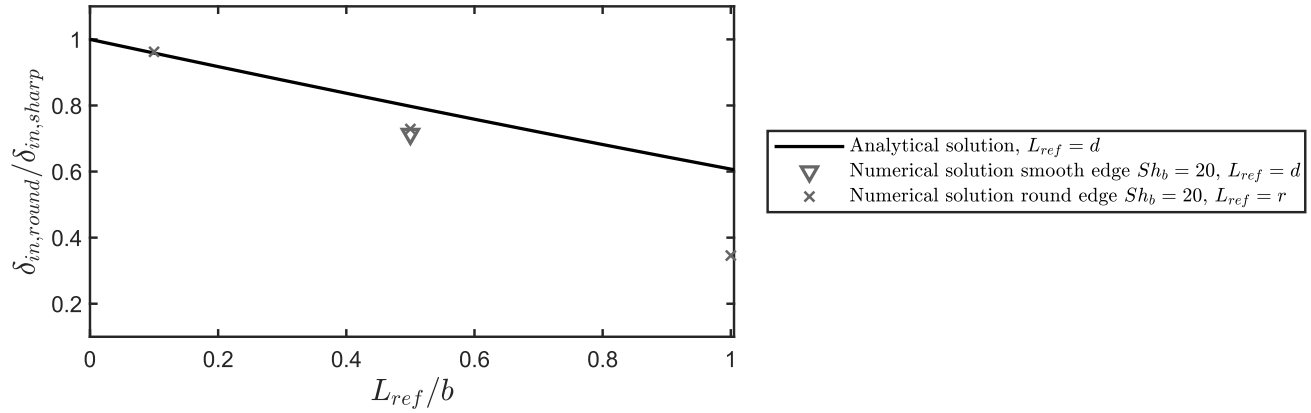

Figure 5: Behavior of $\delta_{in,round}/\delta_{in,sharp}$ as function of the edge rounding L_{ref}/b for $1/\Phi = 10$.

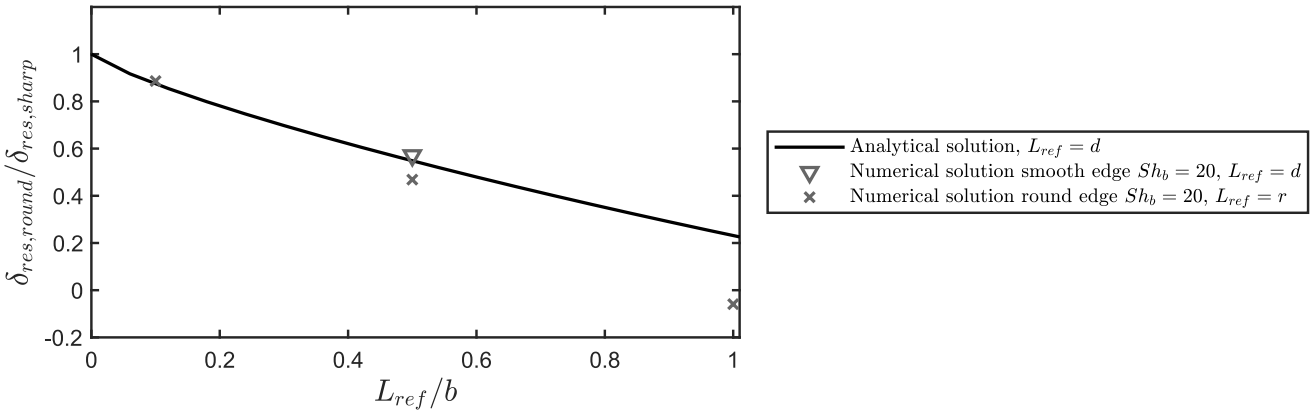

Figure 6: Behavior of $\delta_{res,round}/\delta_{res,sharp}$ as function of the edge rounding L_{ref}/b for $1/\Phi = 10$.

geometry of the edge. In conclusion, it appears that a fair estimation of the edge geometry is necessary to obtain meaningful estimations of the end-correction for slits.

4. Conclusions

This study uses an analytical solution to investigate the influence of the edge geometry on the acoustic behavior of microslit absorbers (MSAs and MSPs). This solution is assessed by the means of numerical solution of the Linearized Navier-Stokes equations[8]. The influence of the edge geometry is investigated by replacing the sharp square edge transition from the slit to the confinement channel by a smooth transition. For high Sh_b numbers, potential flow theory is used in combination with a thin viscous boundary layer approximation. Numerical solutions of the LNSE demonstrate that the analytical model based on the thin boundary layer approximation predicts rounded edges behavior for $r < b$. From this study it emerges that the inertia of the slit is strongly dependent on the porosity. On the contrary, the resistance is weakly dependent on the porosity, indicating that the viscous friction is a local phenomenon, dominated by the edge geometry of the perforation. This is confirmed by the negligible influence of the friction at the walls of the confinement channel, for $\Phi < 0.1$. For sub-millimeter perforations, the manufacturing process will strongly determine the edge geometry. Without taking this edge geometry into account, it is meaningless to use end-corrections for the prediction of the acoustic properties of MSAs.

ACKNOWLEDGMENTS

This work is part of the Marie Skłodowska-Curie Initial Training Network Pollution Know-How and Abatement (POLKA). We gratefully acknowledge the financial support from the European Commission under call H2020-MSCA-ITN-2018 (project number: 813367).

REFERENCES

1. Maa, D.-Y. Theory of microslit absorbers, *Acta Acustica*, **25** (6), 481–485, (2000).

2. Kristiansen, U. R. and Vigran, T. E. On the design of resonant absorbers using a slotted plate, *Applied Acoustics*, **43** (1), 39–48, (1994).

3. Randeberg, R. Adjustable slitted panel absorber, *Acta Acustica united with Acustica*, **88** (4), 507–512, (2002).

4. Zieliński, T. G., Chevillotte, F. and Deckers, E. Sound absorption of plates with micro-slits backed with air cavities: Analytical estimations, numerical calculations and experimental validations, *Applied Acoustics*, **146**, 261–279, (2019).

5. Temiz, M. A., Lopez Arteaga, I., Efraimsson, G., Åbom, M. and Hirschberg, A. The influence of edge geometry on end-correction coefficients in micro perforated plates, *The Journal of the Acoustical Society of America*, **138** (6), 3668–3677, (2015).

6. Billard, R., Tissot, G., Gabard, G. and Versaevel, M. Numerical simulations of perforated plate liners: Analysis of the visco-thermal dissipation mechanisms, *Journal of the Acoustical Society of America*, (2020).

7. Morse, P. M. and Ingard, K. U., *Theoretical acoustics*, Princeton University press (1986).

8. Aulitto, A., Hirschberg, A. and Lopez Arteaga, I. Influence of geometry on end-corrections of slits in microslit absorbers, *Journal of the Acoustical Society of America*, (2021).

9. Henrici, P., *Applied and computational complex analysis, Volume I*, John Wiley & Sons (1974).

10. Hirschberg, L., Schuller, T., Collinet, J., Schram, C. and Hirschberg, A. Analytical model for the prediction of pulsations in a cold-gas scale-model of a solid rocket motor, *Journal of Sound and Vibration*, **419**, 452–468, (2018).

11. Fok, V. Teoreticheskoe issledovanie provodimosti kruglogo otverstiya v peregorodke, postavlennoi poperek truby (theoretical study of the conductance of a circular hole in a partition across a tube), *Doklady Akademii Nauk SSSR (Soviet Physics Doklady)*, **31** (9), 875–882, (1941).

12. Lesser, M. and Lewis, J. Applications of matched asymptotic expansion methods to acoustics. ii. the open-ended duct, *The Journal of the Acoustical Society of America*, **52** (5B), 1406–1410, (1972).

13. Naderyan, V., Raspet, R., Hickey, C. J. and Mohammadi, M. Acoustic end corrections for micro-perforated plates, *The Journal of the Acoustical Society of America*, **146** (4), EL399–EL404, (2019).